Journal of Molecular Graphics and Modelling 72 (2017) 129–135

Contents lists available at ScienceDirect

Journal of Molecular Graphics and Modelling

journal homepage: www.elsevier.com/locate/JMGM

DFT study on the chemical sensing properties of $B_{24}N_{24}$ nanocage toward formaldehyde

Zahra Rostami[a,*], Mansoureh Pashangpour[b], Reza Moradi[c]

[a] Department of Chemistry, Payame Noor University (PNU), P. O. Box, 19395-3697 Tehran, Iran
[b] Department of Physics, Islamshahr Branch, Islamic Azad University, Islamshahr, Iran
[c] Department of Chemistry, Tuyserkan Branch, Islamic Azad University, Tuyserkan, Iran

ARTICLE INFO

Article history:
Received 20 September 2016
Received in revised form
29 November 2016
Accepted 21 December 2016
Available online 26 December 2016

Keywords:
Sensor
Conductivity
DFT
BN nanocage
Recovery time

ABSTRACT

It has been previously shown that the toxic formaldehyde gas (H_2CO) cannot be detected by pristine BC_2N, carbon, and BN nanotubes, BC_3 nanosheet and graphene. Herein, density functional theory calculations were employed to investigate the electronic and structural behavior of a pristine $B_{24}N_{24}$ nanocluster toward H_2CO molecules. It was found that [4,6] B—N bonds of the nanocluster are the most favorable sites for the H_2CO adsorption, compared to the [4,8], and [6,8] ones. When an H_2CO molecule is adsorbed on a [4,6] B—N bond, an energy of about 16.40 kcal/mol is released and the HOMO-LUMO gap of the cluster is decreased from 6.45 to 2.98 eV. Thus, the electrical conductivity of the cluster is significantly increased, indicating that it can produce an electronic noise at the presence of H_2CO molecules. Increasing the number of adsorbed H_2CO molecules, the electrical conductivity more increases. The recovery time for the H_2CO from the surface of $B_{24}N_{24}$ is calculated to be very short (~1.02 s). Also, the UV–vis spectrum shows that the λ_{max} of the $B_{24}N_{24}$ shows a large redshift upon the adsorption process and transfers from the UV to the visible region.

1. Introduction

Formaldehyde (H_2CO) has a high chemical reactivity and thermal stability which is extremely used in several industrial processes [1]. Its concentration is about 1–10 ppb in atmosphere [2]. It is also a highly toxic compound, and its detection is of great importance. Vairavamurthy et al. have published a comprehensive review article on different methods for H_2CO detection such as chromatography, laser induced fluorescence, and Fourier transform infrared absorption spectrophotometry [3]. By advent of nanotechnology, development of chemical sensors was accelerated because of the high surface/volume ratio and unique electronic sensitivity of these materials [4–11]. Numerous chemical nanosensors have been introduced for different gases such as CO, NO, HCN, NO_x, H_2, H_2O, NH_3, etc by experimentalist and theoreticalists [12–19]. Boron nitride (BN) nanomaterials are an important class of nanostructures with wide band gap, special magnetic, optical and electronic properties [20–29]. Serval studies have been focused on the fullerene-like BN nanostructures, nanotubes, and sheets as chemical sensors [30–37].

It has been previously indicated that several nanostructures cannot detect chemicals because of the weak interaction and small charge transfer [38–45]. To overcome this problem several methods have been introduced including chemical functionalization, doping, making defects in the structure of potential sensor, and so on [46–51]. For example, it has been shown that H_2CO can be detected by N-doped single-walled carbon nanotubes, Si-doped BC_3 graphenes, Si-doped BN, and BC_2N nanotubes, while none of these materials in their pristine form cannot detect the gas [43,44]. Meanwhile, structural engineering is difficult and an expensive process. Thus, it is of great importance to introduce a nanomaterial that can detect the chemicals such as H_2CO in its pristine form.

Oku et al. [52] have reported the synthesis of $B_{24}N_{24}$ nanoclusters which includes hexagonal, tetragonal, and octagonal rings, obeying from the isolated tetragonal rule. Different properties and applications of this nanocluster have been studied by different groups [53–56]. It has been shown that the hydrogen storage capability of the $B_{24}N_{24}$ nanoclusters will increase by Al doping [53]. Koi et al. indicated that Li-endohedral $B_{24}N_{24}$ nanocluster ($Li@B_{24}N_{24}$) significantly has higher hydrogen storage capability compared to the pristine cage [56]. Herein, we investigate the capability of this nanostructure as a chemical gas sensor for H_2CO gas by means of density functional theory (DFT) calculations.

* Corresponding author.
E-mail address: zahrarostami.pnu@gmail.com (Z. Rostami).

http://dx.doi.org/10.1016/j.jmgm.2016.12.013
1093-3263/

Table 1
Calculated adsorption energy (E_{ad}, kcal/mol), Gibbs free energy change (ΔG, kcal/mol), HOMO, LUMO energies, HOMO-LUMO energy gap (E_g), and Fermi level energy (E_F) of formaldehyde adsorbed on the $B_{24}N_{24}$. Energy of electronic properties is in eV. See Figs. 1–3.

system	E_{ad}	ΔG	LUMO	E_F	HOMO	E_g	[a] ΔE_g (%)	[b] Q_T (|e|)
$B_{24}N_{24}$	–	–	−0.94	−4.16	−7.39	6.45	–	–
A	−0.23	−0.18	−0.90	−4.09	−7.28	6.38	−1.08	0.04
B	−0.17	−0.13	−0.81	−4.01	−7.21	6.40	−0.77	0.03
C	−16.40	−15.05	−3.63	−5.12	−6.61	2.98	−53.7	0.41
D	−15.06	−14.51	−3.52	−5.06	−6.60	3.08	−52.2	0.39
E	−12.31	−10.97	−3.56	−5.06	−6.57	3.01	−53.3	0.33

[a] ΔE_g (%) is the percentage of the E_g change in the BN cage after the adsorption of H_2CO.
[b] Q_T is defined as the total NBO charge on the formaldehyde.

Table 2
Calculated adsorption energy per molecule (E_{ad}, kcal/mol), HOMO, LUMO energies, HOMO-LUMO energy gap (E_g), and Fermi level energy (E_F) of different number formaldehyde adsorbed on the $B_{24}N_{24}$. Energy of electronic properties is in eV. See Fig. 5. The ΔE_g (%) is the percentage of E_g change in the BN cage after the adsorption of H_2CO molecules.

system	E_{ad}	LUMO	E_F	HOMO	E_g	ΔE_g (%)
$B_{24}N_{24}$	–	−0.94	−4.16	−7.39	6.45	–
2-H_2CO	−16.43	−3.71	−5.10	−6.50	2.79	−56.7
3-H_2CO	−15.45	−3.79	−5.13	−6.48	2.69	−58.2
4-H_2CO	−16.48	−3.85	−5.15	−6.46	2.61	−59.2

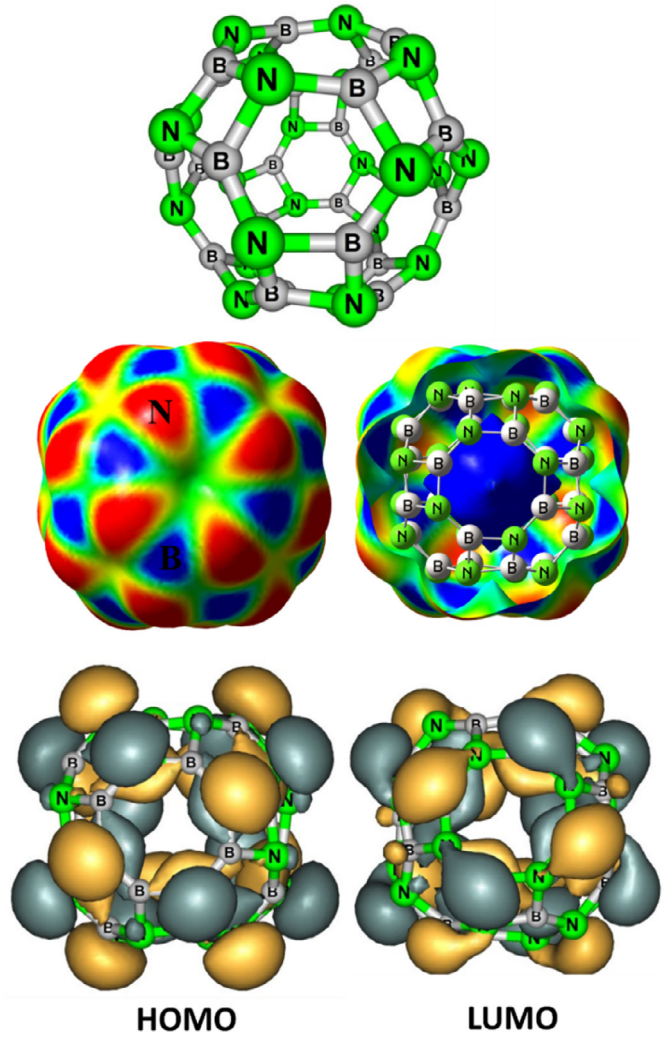

Fig. 1. Optimized structure of $B_{24}N_{24}$ nanocluster, and its outer and inner MEP plots, plus the HOMO and LUMO profiles. Color ranges, in a.u.: blue, more positive than 0.015; green, between 0.015 and 0; yellow, between 0 and −0.015; red, more negative than −0.015. (For interpretation of the references to colour in this figure legend, the reader is referred to the web version of this article.)

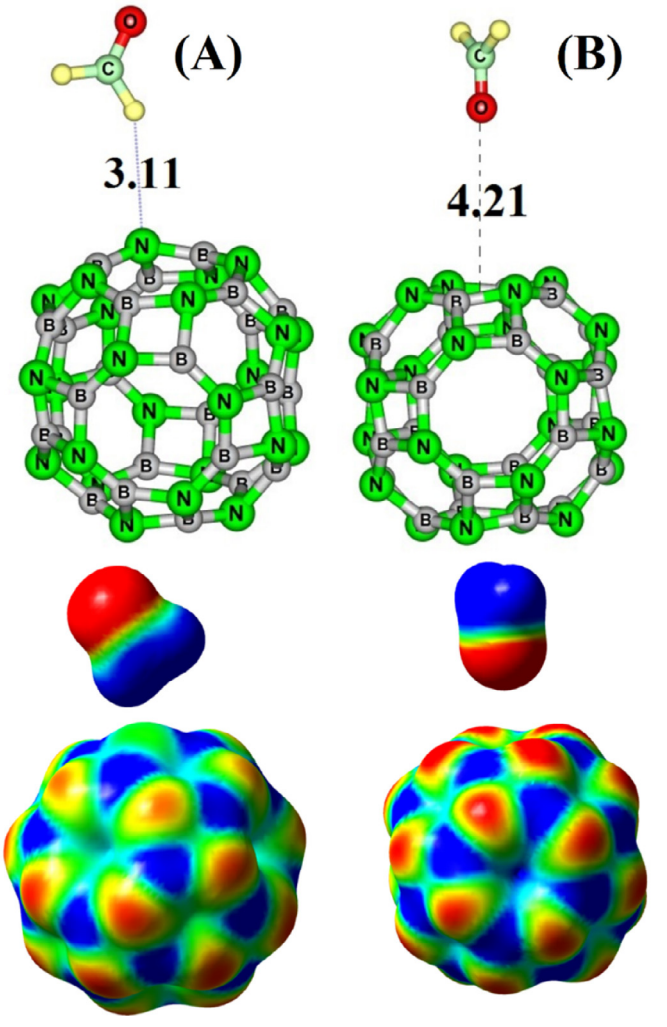

Fig. 2. Optimized structures for physisorption of H_2CO molecule on the $B_{24}N_{24}$ nanocluster and their MEP plots. Distance in Å. Color ranges, in a.u.: blue, more positive than 0.015; green, between 0.015 and 0; yellow, between 0 and −0.015; red, more negative than −0.015. (For interpretation of the references to colour in this figure legend, the reader is referred to the web version of this article.)

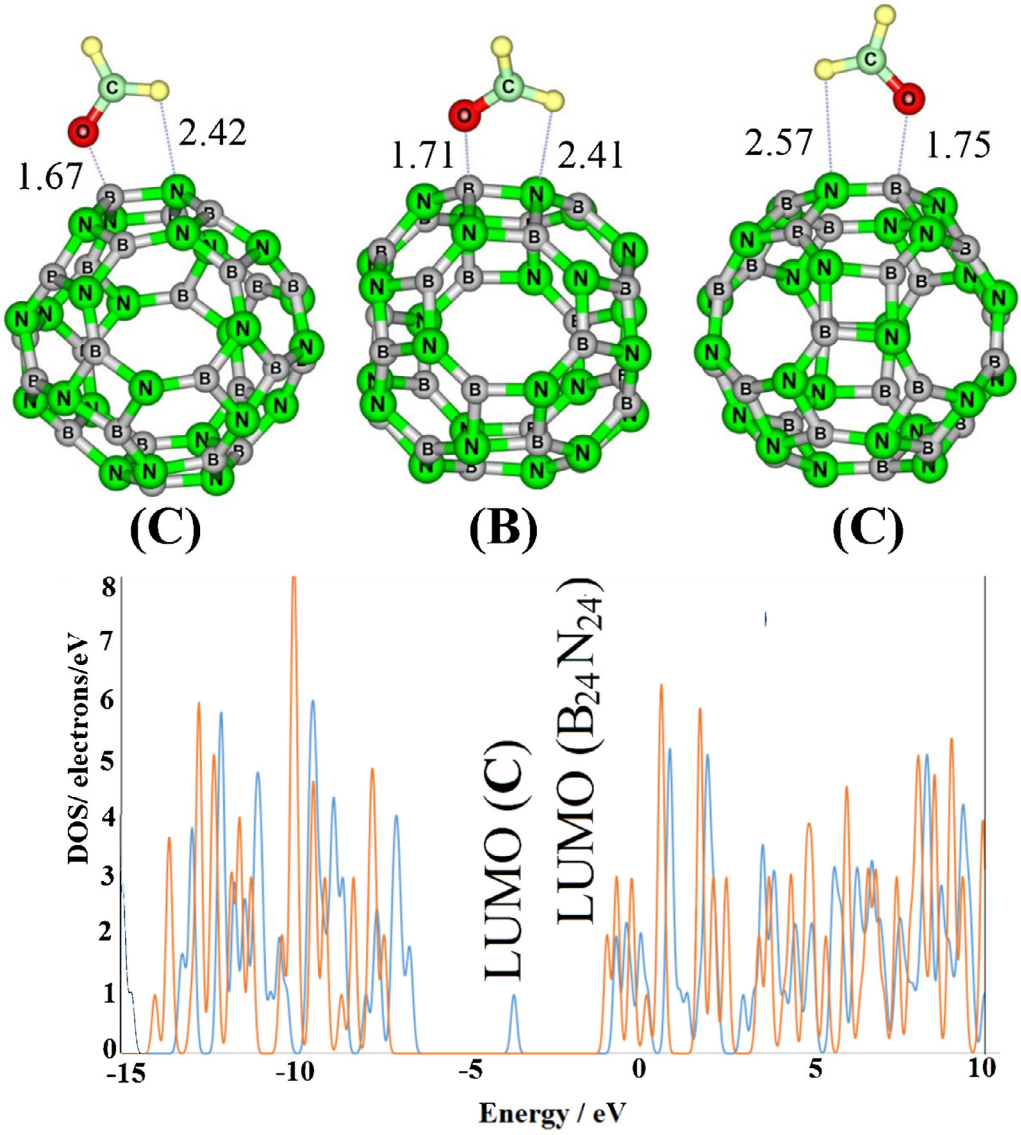

Fig. 3. Optimized structures for chemisorption of H_2CO molecule on the $B_{24}N_{24}$ nanocluster. Distances in Å. DOS plots for pristine $B_{24}N_{24}$ nanocluster (red line) and complex **C** (blue line). (For interpretation of the references to colour in this figure legend, the reader is referred to the web version of this article.)

2. Computational details

Geometry optimizations, energy calculations, natural bond orbitals (NBO) [57], molecular electrostatic potential (MEP) [58] and density of states (DOS) analyses were performed on a $B_{24}N_{24}$ nanocluster and different $H_2CO/B_{24}N_{24}$ complexes using the B3LYP functional [59,60] augmented with an empirical dispersion term [61] (B3LYP-D) with 6–31G(d) basis set. The B3LYP has been demonstrated to be a reliable and commonly employed density functional in the study of different nanomaterials [62–65]. It has been also indicated that the B3LYP provides an efficient and robust basis for calculations of III–V semiconductors [66]. The GAMESS suite of program was used to perform all the calculations. [67]. GaussSum program was used to get the DOS plots [68]. We defined the adsorption energy as:

$$E_{ad} = E(H_2CO/B_{24}N_{24}) - E(B_{24}N_{24}) - E(H_2CO) + E_{BSSE} \quad (1)$$

where $E(H_2CO/B_{24}N_{24})$ corresponds to the energy of the $H_2CO/B_{24}N_{24}$ complex, $E(B_{24}N_{24})$ is the energy of the isolated $B_{24}N_{24}$, $E(H_2CO)$ is the energy of a single H_2CO molecule, and E_{BSSE} is the energy of the basis set superposition error. We used the counterpoise method of Boys and Bernardi to calculate the E_{BSSE} [69]. Fermi level is approximately defined to be in the middle of the highest occupied molecular orbital (HOMO) and the lowest unoccupied molecular orbital (LUMO) energy gap (E_g). The E_g is connected to the population of conduction electrons (N) by the below equation [70]:

$$N = AT^{3/2}\exp(-E_g/2kT) \quad (2)$$

where k is the Boltzmann's constant and A (electrons/$m^3K^{3/2}$) is a constant. This procedure has been frequently employed to display the nanostructure sensitivity toward a chemical and has shown a good agreement with the experimental results [70].

3. Results and discussion

3.1. The $B_{24}N_{24}$ properties

The equilibrium structure of $B_{24}N_{24}$ is displayed in Fig. 1 which follows the experimentally shown symmetry and geometry [52]. Oku et al. have demonstrated that their synthesized $B_{24}N_{24}$ cluster has 6 octagons, 8 hexagons, and 12 tetragons with *O* symmetry

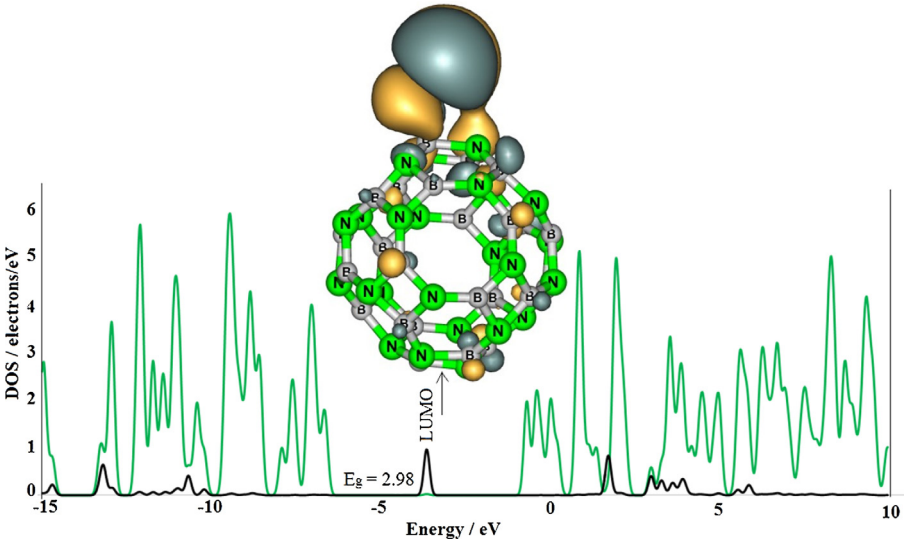

Fig. 4. The partial DOS plot for complex **C** in which the black line shows the contribution of H_2CO molecule and the green line shows that of $B_{24}N_{24}$ cluster. Also, the LUMO profile of this complex indicates that the LUMO is shifted on the H_2CO molecule in good agreement with its energy shift. (For interpretation of the references to colour in this figure legend, the reader is referred to the web version of this article.)

[52]. In the structure of $B_{24}N_{24}$ nanocluster, three different B-N bonds can be found; namely, [4,8], [4,6], [6,8] bonds. The numbers 4, 6, and 8 designate the tetragon, hexagon, and octagon, respectively. The order of magnitude for the length of these bonds is as [4,6] (∼1.51 Å) > [4,8] (∼1.47 Å) > [6,8] (∼1.42 Å). The bond which is shared between smaller rings has a larger bondlength due to the higher strain. Table 1 displays that the HOMO and LUMO levels of $B_{24}N_{24}$ lie at −7.39 and −0.94 eV, respectively, which produce an E_g of 6.45 eV. Fig. 1 indicates that the HOMO and LUMO more localized on the N and B sites, respectively.

The MEP plot (Fig. 1) demonstrates that N and B atoms are negatively and positively charged and the center of the rings seems to be compensated. Also, the core of the cage is positively charged which may be due to the fact that the hybridization of the N atoms is approximately sp^3 and their lone pairs are outside of the surface. Thus, the N atoms are slightly projected out of the surface and the B atoms are oriented toward the inside, resulting in a positive core for the cage. The NBO analysis indicates a partially ionic character for B-N bonds in which a charge of 0.47 *e* transfers from the boron to nitrogen atoms.

3.2. The adsorption of H_2CO on the $B_{24}N_{24}$

We probed a number of distinct initial structures for the adsorption of H_2CO on the $B_{24}N_{24}$. The molecule is located form its H atoms on the N atoms of the cluster, from the O atom on the center of rings or on the B sites, locating the molecule on the B-N bonds from different positions and so on. Finally, we found 5 local minima with positive frequencies which were categorized into two classes including physisorption and chemisorption. In the next part of the article, we explain and consider these classes.

3.2.1. Physisorption

We predicted two $H_2CO/B_{24}N_{24}$ complexes (Fig. 2) with weak interaction between the H_2CO and $B_{24}N_{24}$. In one complex (**A**), the H_2CO is relaxed from one H atom on an N atom of the cluster in the distance of 3.11 Å. The calculated adsorption energy is about −0.23 kcal/mol, which shows a weak interaction. The predicted change of Gibbs free energy (ΔG) at room temperature is somewhat less negative (∼−0.18 kcal/mol) due to the entropic effect. The charge distribution in Fig. 2 shows that there is a node between the H_2CO and $B_{24}N_{24}$, approving the weak interaction. Table 1 reveals that the electronic properties HOMO, LUMO, E_g, and Fermi level of $B_{24}N_{24}$ nanocluster are not affected by the adsorption process. In the other physisorption state, the H_2CO molecule is relaxed on the center of an octagonal ring at the distance of 4.21 Å (Fig. 2**B**) and the adsorption energy is about −0.17 kcal/mol (ΔG∼−0.13 kcal/mol). Similar to the complex **A**, a node can be seen between the H_2CO and $B_{24}N_{24}$ in the charge distribution plot (Fig. 2). Table 1 indicates that the electronic properties of this complex are similar to those of the pure $B_{24}N_{24}$ nanocluster. Consequently, these adsorption processes are not appropriate for the detection of H_2CO by $B_{24}N_{24}$ nanocluster.

3.2.2. Chemisorption

When the H_2CO molecule is located on the each of three types of B-N bonds, its oxygen atom relaxes on the B atom and one of H atoms forms a bond with the N atom as shown in Fig. 3. The order of calculated adsorption energies for these bonds is as [4,6] (∼−16.40), **C** > [4,8] (∼ −15.06), **D** > [6,8] (∼−12.31), **E,** Table 1, kcal/mol. The complex **C** is the most stable one in which the distances of B···O and N···H are about 1.67 and 2.42 Å, respectively. It seems that the bonds which are more strained are more reactive, and give more negative adsorption energies. In the complex **C** (the most stable) the length of adsorbing [4,6] bond is increased from 1.51 to 1.59 Å, and, also, B atom projected out of the surface showing a local deformation due to a strong interaction.

The vibrational frequency analysis indicates that the stretching mode of C—O in the free H_2CO molecule is about 1850 cm^{-1} which decreases to 1620 cm^{-1} in the complex **C**. This shows that this bond weakens due to a charge transfer from the lone pairs of O atom to the empty p-orbital of the B atom and a π-backbonding from the cage to the C—O empty π^* orbital. The calculations demonstrate that the bondlength of C—O is increased from 1.21 to 1.25 Å, confirming the vibrational frequency reduction. Overall, an NBO charge of 0.41 e is transferred from the H_2CO molecule to the $B_{24}N_{24}$ cage.

3.2.2.1. The electronic properties. Herein, our main purpose is to investigate the ability of the $B_{24}N_{24}$ in detection of H_2CO gas. Besides the expensive experimental techniques, several theoretical methods have been employed to study the sensing behavior of nanostructures toward different toxic gases [71–75]. One of the most prevalent theoretical methods [76–78] is based on the change of E_g of adsorbent upon the gas adsorption as shown by Eq. (2). As

shown in Table 1, the electronic properties of the $B_{24}N_{24}$ are considerably perturbed after H_2CO adsorption. Especially, the LUMO level shifts to lower energies by about 2.69 eV which reduces the E_g from 6.45 in the bare cage to 2.98 eV in the complex **C**.

The DOS plots of the bare cage and complex **C** (in one diagram, Fig. 3) demonstrate that the HOMO level slightly shifts to higher energies and the LUMO strongly to lower energies, thereby, reducing the E_g. The partial DOS of the complex **C** in Fig. 4 reveals that after the adsorption of the H_2CO molecule a new state is appeared at −3.63 eV which is mainly comes from the H_2CO molecule. Also, the LUMO profile (Fig. 4) of the complex **C** shows that the H_2CO mainly contributes in the LUMO level. The Fermi level is also significantly stabilized (by about 0.96 eV). Based on Eq. 2, the large reduction of the E_g significantly increases the electrical conductivity of the $B_{24}N_{24}$ nanocluster. Thus, this cluster can produce an electrical noise in the presence of H_2CO gases and may be utilized in the H_2CO-sensor devices. Our UV–vis calculations show that the pristine $B_{24}N_{24}$ cluster has a λ_{max} at 219 nm in the UV region which makes the cluster colorless. But after the attaching H_2CO molecule to the cluster the λ_{max} is shifted to the visible region (∼524 nm), thus, the complex will be colored. The λ_{max} shift to larger wavelengths (redshift) is in good agreement with the E_g reduction. This characteristic can be used for detection of H_2CO in a solution environment.

3.2.2.2. Recovery time. The recovery of the sensor form the adsorbed molecules is an essential issue. Experimentally the recovery of a sensor is performed by heating to higher temperatures or by exposure to UV light [79]. The recovery time of $B_{24}N_{24}$ nanocluster for H_2CO gas can be predicted from the following formula of transition theory:

$$\tau = \upsilon^{-1}\exp(-E_{ad}/kT) \quad (5)$$

where k is the Boltzmann's constant (∼1.99 * 10^{-3} kcal/mol K), T is temperature, and υ the attempt frequency. If we use the attempt frequency (∼10^{12} s^{-1}) which has been used to the recovery of carbon nanotubes at room temperature [80], the recovery time of H_2CO from the surface of $B_{24}N_{24}$ will be about 1.02 s. This indicates that the $B_{24}N_{24}$ senor benefits from a short recovery time. As a comparison, the recovery time of the SnO_2 microspheres and Er-doped In_2O_3 nanotubes as a chemical sensor for H_2CO is about are 25 and 38 *s*, respectively [81,82]. As another example, it has been reported that for NO_2 desorption from the surface of N-doped carbon nanotubes, the recovery time is about 9 ms which is excellent [38]. However, the recovery time of $B_{24}N_{24}$ seems to be short enough to be used in a sensor device. Compared to the pristine $B_{24}N_{24}$, it has been shown that pristine BC_2N [40], carbon [83], and BN nanotubes [43], BC_3 nanosheets [44] and graphene [84] cannot detect the H_2CO gas and a structural manipulation with doping process is required to improve the sensitivity. In the pristine form, BeO nanotubes show a decrease of 40.5% in E_g upon the H_2CO molecule which shows good performance but its adsorption energy (−25.1 kcal/mol) is more negative than that of $B_{24}N_{24}$ which largely prolongs the recovery time [85]. Also, the AlN nanotubes which have been introduced as chemical sensor for H_2CO suffer from a long recovery time because of a more negative adsorptions energy of −1.3 eV [86]. It has been previously reported that adsorption energy of about −1.0 eV corresponds to a recovery time of 12 h [80].

3.2.2.3. Effect of concentration. We investigated the concentration of the H_2CO molecules (or gas pressure) on the sensitivity and adsorption properties of the BN cluster. To this aim, assuming the [4,6] bonds as the most favorable adsorption sites, the adsorption of second, third, and fourth H_2CO molecule is investigated and the results are summarized in Table 2 and depicted in Fig. 5. To reduce the steric repulsion between the adsorbate molecules, we choose the adsorption sites to be far from the others as possible. The adsorption energy per molecule becomes slightly more negative for second, third and fourth H_2CO molecule (Table 2). Compared to the adsorption energy change which is negligible, the electronic properties are more affected by the increase of the number of H_2CO molecules. Overall, the HOMO and LUMO shifts to lower energies and the E_g becomes smaller by increasing the number of H_2CO molecules. For example, when four H_2CO molecules are adsorbed on the cluster, the ΔE_g is increased to 59.2% which is larger by about 5.50% from the ΔE_g in the complex **C**.

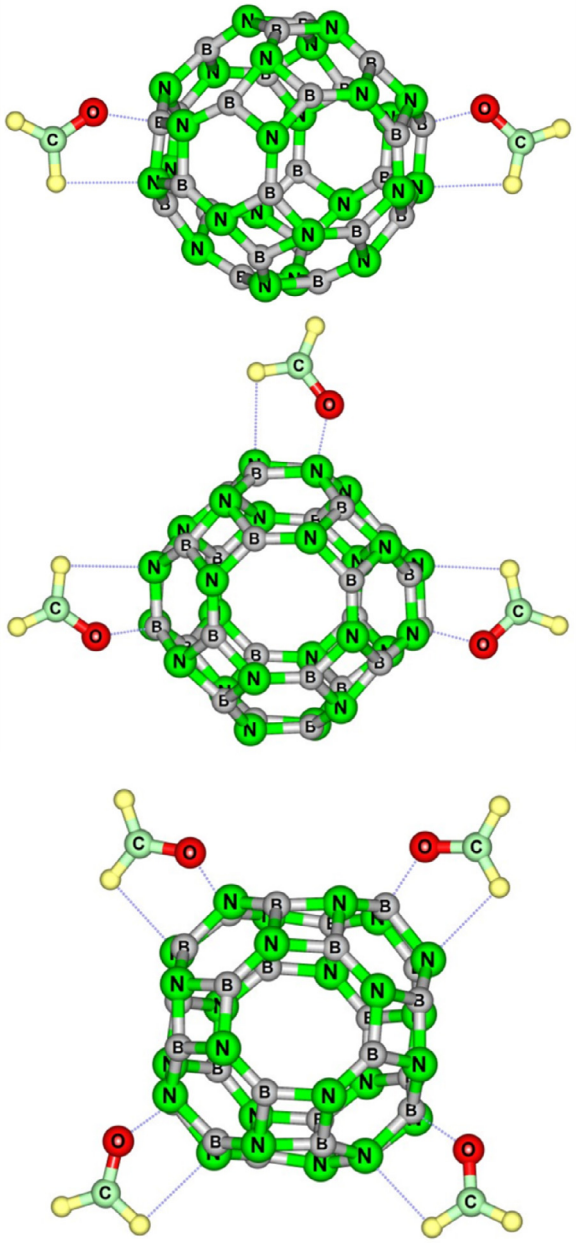

Fig. 5. Optimized structures for the adsorption of 2, 3, and 4 H_2CO molecules o the $B_{24}N_{24}$ nanocluster.

4. Conclusions

Using III-Nitride nanostructures is of great importance in gas sensing devices. Here, using DFT calculations, the electronic and structural behaviors of a $B_{24}N_{24}$ nanocluster toward

H_2CO molecules were investigated. Two adsorption ways are predicted; namely, physisorption and chemisorption with the adsorption energies in the range of −0.17 to −0.23, and −12.31 to −16.40 kcal/mol, respectively. It is found that upon the chemisorption process the electrical conductivity of the cluster is significantly increased because of the appearance of a new state within its E_g. Thus, the $B_{24}N_{24}$ can produce an electronic signal at the presence of H_2CO molecules which is proportional to the concentration of the gas. The recovery time is calculated to be very short (∼1.02 s). Also, the BN cluster can be used in the pristine form and no further expensive structural manipulation is required to improve its sensitivity. Our modelling results indicate that $B_{24}N_{24}$ cluster possesses structural and electronic properties which are quit promising for its application in gas detection such an H_2CO sensing device(s)

References

[1] Y. Mine, N. Melander, D. Richter, D.G. Lancaster, K.P. Petrov, F.K. Tittel, Detection of formaldehyde using mid-infrared difference-frequency generation, Appl. Phys. B 65 (1997) 771–774.
[2] P. Dingle, P. Franklin, Formaldehyde levels and the factors affecting these levels in homes in Perth Western Australia, Indoor Built Environ. 11 (2002) 111–116.
[3] A. Vairavamurthy, J.M. Roberts, L. Newman, Methods for determination of low molecular weight carbonyl compounds in the atmosphere: a review, Atmos. Environ. 26 (1992) 1965–1993.
[4] A.L. Petranovska, N.V. Abramov, S.P. Turanska, P.P. Gorbyk, A.N. Kaminskiy, N.V. Kusyak, Adsorption of cis-dichlorodiammineplatinum by nanostructures based on single-domain magnetite, J. Nanostruct. Chem. 5 (2015) 275–285.
[5] J. Beheshtian, M. Noei, H. Soleymanabadi, A.A. Peyghan, Ammonia monitoring by carbon nitride nanotubes: a density functional study, Thin Solid Films 534 (2013) 650–654.
[6] M. Noei, M. Ebrahimikia, Y. Saghapour, M. Khodaverdi, A.A. Salari, N. Ahmadaghaei, Removal of ethyl acetylene toxic gas from environmental systems using AlN nanotube, J. Nanostruct. Chem. 5 (2015) 213–217.
[7] A.S. Kornyushchenko, A.H. Jayatissa, V.V. Natalich, V.I. Perekrestov, Two step technology for porous ZnO nanosystem formation for potential use in hydrogen gas sensors, Thin Solid Films 604 (2016) 48–54.
[8] A.M. Attaran, S. Abdol-Manafi, M. Javanbakht, M. Enhessari, Voltammetric sensor based on Co_3O_4/SnO_2 nanopowders for determination of diltiazem in tablets and biological fluids, J. Nanostruct. Chem. 6 (2016) 121–128.
[9] L. Mahdavian, Simulation of SnO_2/WO_3 nanofilms for alcohol of gas sensor based on metal dioxides: MC and LD studies, J. Nanostruct. Chem. 3 (2012) 1–7.
[10] R.B. dos Santos, F. de Brito Mota, R. Rivelino, A. Kakanakova-Georgieva, G.K. Gueorguiev, Van der Waals stacks of few-layer h-AlN with graphene: an ab initio study of structural, interaction and electronic properties, Nanotechnology 27 (2016) 145601–145609.
[11] R.B. dos Santos, R. Rivelino, F. de Brito Mota, A. Kakanakova-Georgieva, G.K. Gueorguiev, Feasibility of novel (H 3C) n X (SiH 3) 3- n compounds (X = B, Al, Ga, In): structure, stability, reactivity, and Raman characterization from ab initio calculations, Dalton Trans. 44 (2015) 3356–3366.
[12] J. Beheshtian, A.A. Peyghan, Z. Bagheri, M. Kamfiroozi, Interaction of small molecules (NO, H_2, N_2, and CH_4) with BN nanocluster surface, Struct. Chem. 23 (2012) 1567–1572.
[13] A.A. Peyghan, M. Noei, M.B. Tabar, A large gap opening of graphene induced by the adsorption of CO on the Al-doped site, J. Mol. Model. 19 (2013) 3007–3014.
[14] D. Berger, A.P. de Moura, L.H. Oliveira, W.B. Bastos, F.A. La Porta, I.L.V. Rosa, M.S. Li, S.M. Tebcherani, E. Longo, J.A. Varela, Improved photoluminescence emission and gas sensor properties of ZnO thin films, Ceram. Int. 42 (2016) 13555–13561.
[15] J. Beheshtian, A.A. Peyghan, Z. Bagheri, Sensing behavior of Al-rich AlN nanotube toward hydrogen cyanide, J. Mol. Model. 19 (2013) 2197–2203.
[16] M.T. Baei, A.A. Peyghan, Z. Bagheri, A computational study of AlN nanotube as an oxygen detector, Chin. Chem. Lett. 23 (2012) 965–968.
[17] H. Manap, K. Suzalina, M.S. Najib, A potential development of breathing gas sensor using an open path fibre technique, Microelectron. Eng. 164 (2016) 59–62.
[18] A.A. Peyghan, S.F. Rastegar, N.L. Hadipour, DFT study of NH_3 adsorption on pristine, Ni-and Si-doped graphynes, Phys. Lett. A 378 (2014) 2184–2190.
[19] L. Yuan, M. Hu, Y. Wei, W. Ma, Enhanced NO_2 sensing characteristics of Au modified porous silicon/thorn-sphere-like tungsten oxide composites, Appl. Surf. Sci. 389 (2016) 824–834.
[20] J. Beheshtian, H. Soleymanabadi, A.A. Peyghan, Z. Bagheri, A DFT study on the functionalization of a BN nanosheet with PC-X,(PC = phenyl carbamate, X = OCH_3, CH_3, NH_2, NO_2 and CN), Appl. Surf. Sci. 268 (2012) 436–441.
[21] S.J. Mahdizadeh, E.K. Goharshadi, G. Akhlamadi, Thermo-mechanical properties of boron nitride nanoribbons: a molecular dynamics simulation study, J. Mol. Graphics Modell. 68 (2016) 1–13.
[22] J. Beheshtian, A.A. Peyghan, Z. Bagheri, Arsenic interactions with a fullerene-like BN cage in the vacuum and aqueous phase, J. Mol. Model. 19 (2013) 833–837.
[23] J. Beheshtian, A.A. Peyghan, Z. Bagheri, Functionalization of BN nanosheet with N_2H_4 may be feasible in the presence of Stone–Wales defect, Struct. Chem. 24 (2013) 1565–1570.
[24] W.-Y. Wang, N.-N. Ma, C.-H. Wang, M.-Y. Zhang, S.-L. Sun, Y.-Q. Qiu, Enhancement of second-order nonlinear optical response in boron nitride nanocone: Li-doped effect, J. Mol. Graphics Modell. 48 (2014) 28–35.
[25] J. Beheshtian, M.B. Tabar, Z. Bagheri, A.A. Peyghan, Exohedral and endohedral adsorption of alkaline earth cations in BN nanocluster, J. Mol. Model. 19 (2013) 1445–1450.
[26] M.T. Baei, A.A. Peyghan, Z. Bagheri, A density functional theory study on acetylene-functionalized BN nanotubes, Struct. Chem. 24 (2013) 1007–1013.
[27] A.V. Moradi, A.A. Peyghan, S. Hashemian, M.T. Baei, Theoretical study of thiazole adsorption on the (6, 0) zigzag single-walled boron nitride nanotube, Bull. Korean Chem. Soc. 33 (2012) 3285–3292.
[28] S.J. Mahdizadeh, E.K. Goharshadi, G. Akhlamadi, Thermo-mechanical properties of boron nitride nanoribbons: a molecular dynamics simulation study, J. Mol. Graphics Modell. 68 (2016) 1–13.
[29] R. Freitas, G.K. Gueorguiev, F. de Brito Mota, C. de Castilho, S. Stafström, A. Kakanakova-Georgieva, Reactivity of adducts relevant to the deposition of hexagonal BN from first-principles calculations, Chem. Phys. Lett. 583 (2013) 119–124.
[30] J. Beheshtian, Z. Bagheri, M. Kamfiroozi, A. Ahmadi, Toxic CO detection by $B_{12}N_{12}$ nanocluster, Microelectron. J. 42 (2011) 1400–1403.
[31] Z.-Y. Deng, J.-M. Zhang, K.-W. Xu, Adsorption of SO_2 molecule on doped (8, 0) boron nitride nanotube: a first-principles study, Phys. E 76 (2016) 47–51.
[32] J. Beheshtian, A.A. Peyghan, Z. Bagheri, Detection of phosgene by Sc-doped BN nanotubes: a DFT study, Sens. Actuators B: Chem. (2012) 846–852.
[33] P. Srivastava, N.K. Jaiswal, V. Sharma, First-principles investigation of armchair boron nitride nanoribbons for sensing PH_3 gas molecules, Superlattices Microstruct. 73 (2014) 350–358.
[34] A.A. Peyghan, H. Soleymanabadi, Computational study on ammonia adsorption on the $X_{12}Y_{12}$ nanoclusters (X = B Al and Y = N, P), Curr. Sci. 108 (2015) 00113891.
[35] P. Srivastava, V. Sharma, N.K. Jaiswal, Adsorption of $COCl_2$ gas molecule on armchair boron nitride nanoribbons for nano sensor applications, Microelectron. Eng. 146 (2015) 62–67.
[36] M. Samadizadeh, A.A. Peyghan, S.F. Rastegar, Sensing behavior of BN nanosheet toward nitrous oxide: a DFT study, Chin. Chem. Lett. 26 (2015) 1042–1045.
[37] Y.-q. Zhang, Y.-J. Liu, Y.-l. Liu, J.-x. Zhao, Boosting sensitivity of boron nitride nanotube (BNNT) to nitrogen dioxide by Fe encapsulation, J. Mol. Graphics Modell. 51 (2014) 1–6.
[38] L. Bai, Z. Zhou, Computational study of B-or N-doped single-walled carbon nanotubes as NH_3 and NO_2 sensors, Carbon 45 (2007) 2105–2110.
[39] A.A. Peyghan, M.T. Baei, M. Moghimi, S. Hashemian, Theoretical study of phenol adsorption on pristine, Ga-doped, and Pd-decorated (6, 0) zigzag single-walled boron phosphide nanotubes, J. Cluster Sci. 24 (2012) 49–60.
[40] H.-p. Zhang, X.-g. Luo, X.-y. Lin, Y.-p. Zhang, P.-p. Tang, X. Lu, Y. Tang, Band structure of graphene modulated by Ti or N dopants and applications in gas sensoring, J. Mol. Graphics Modell. 61 (2015) 224–230.
[41] A.A. Peyghan, H. Soleymanabadi, Z. Bagheri, Theoretical study of carbonyl sulfide adsorption on Ag-doped SiC nanotubes, J. Iran. Chem. Soc. 12 (2015) 1071–1076.
[42] A.A. Peyghan, M.B. Tabar, J. Kakemam, NH3 on a BC3 nanotube: effect of doping and decoration of aluminum, J. Mol. Model. 19 (2013) 3793–3798.
[43] R. Wang, R. Zhu, D. Zhang, Adsorption of formaldehyde molecule on the pristine and silicon-doped boron nitride nanotubes, Chem. Phys. Lett. 467 (2008) 131–135.
[44] J. Beheshtian, A.A. Peyghan, M. Noei, Sensing behavior of Al and Si doped BC_3 graphenes to formaldehyde, Sens. Actuators B: Chem. 181 (2013) 829–834.
[45] A. Ahmadi Peyghan, A. Omidvar, N.L. Hadipour, Z. Bagheri, M. Kamfiroozi, Can aluminum nitride nanotubes detect the toxic NH_3 molecules? Phys. E 44 (2012) 1357–1360.
[46] P. Pannopard, P. Khongpracha, M. Probst, J. Limtrakul, Gas sensing properties of platinum derivatives of single-walled carbon nanotubes: a DFT analysis, J. Mol. Graphics Modell. 28 (2009) 62–66.
[47] H.Y. He, J. Fei, J. Lu, Sm-doping effect on optical and electrical properties of ZnO films, J. Nanostruct. Chem. 5 (2015) 169–175.
[48] A. Ahmadi Peyghan, N.L. Hadipour, Z. Bagheri, Effects of Al doping and double-antisite defect on the adsorption of HCN on a BC_2N nanotube: density functional theory studies, J. Phys. Chem. C 117 (2013) 2427–2432.
[49] M. Rezaei-Sameti, E. Samadi Jamil, The adsorption of CO molecule on pristine, As, B, BAs doped (4, 4) armchair AlNNTs: a computational study, J. Nanostruct. Chem. 6 (2016) 197–205.
[50] C. Chen, K. Xu, X. Ji, L. Miao, J. Jiang, Enhanced adsorption of acidic gases (CO_2, NO_2 and SO_2) on light metal decorated graphene oxide, Phys. Chem. Chem. Phys. 16 (2014) 11031–11036.
[51] F. Shirini, M. Abedini, S. Zamani, H. Fallah Moafi, Introduction of W-doped ZnO nanocomposite as a new and efficient nanocatalyst for the synthesis of biscoumarins in water, J. Nanostruct. Chem. 5 (2015) 123–130.
[52] T. Oku, A. Nishiwaki, I. Narita, M. Gonda, Formation and structure of $B_{24}N_{24}$ clusters, Chem. Phys. Lett. 380 (2003) 620–623.

[53] Z. Ma, Y. Zhang, F. Li, H. Chen, Comparative study of H 2 adsorption on B_{24} N_{24}, $Al_{24}N_{24}$ and $B_{12}Al_{12}N_{24}$ clusters, Comput. Mater. Sci. 117 (2016) 71–75.
[54] N. Koi, T. Oku, K. suaki Suganuma, Effects of endohedral element in $B_{24}N_{24}$ clusters on hydrogenation studied by molecular orbital calculations, Phys. E: Low-dimensional Syst. Nanostruct. 29 (2005) 541–545.
[55] G.M. Rouzbehani, A. Boshra, A. Seif, B24N24 nanocages: a GIAO density functional theory study of 14N and 11 B nuclear magnetic shielding and electric field gradient tensors, Monatsh. Chem.-Chem. Mon. 140 (2009) 255–263.
[56] M. Mileev, S. Kuzmin, V. Parfenyuk, Ab initio calculations of structure and stability of small boron nitride clusters, J. Struct. Chem. 47 (2006) 1016–1021.
[57] F. Weinhold, C.R. Landis, Natural bond orbitals and extensions of localized bonding concepts, Chem. Educ. Res. Pract. 2 (2001) 91–104.
[58] P. Politzer, J.S. Murray, The fundamental nature and role of the electrostatic potential in atoms and molecules, Theor. Chem. Acc. 108 (2002) 134–142.
[59] A.D. Becke, Density-functional thermochemistry. III. The role of exact exchange, J. Chem. Phys. 98 (1993) 5648–5652.
[60] C. Lee, W. Yang, R.G. Parr, Development of the Colle-Salvetti correlation-energy formula into a functional of the electron density, Phys. Rev. B 37 (1988) 785.
[61] S. Grimme, Accurate description of van der Waals complexes by density functional theory including empirical corrections, J. Comput. Chem. 25 (2004) 1463–1473.
[62] A. Arab, M. Habibzadeh, Theoretical study of geometry, stability and properties of Al and AlSi nanoclusters, J. Nanostruct. Chem. 6 (2016) 111–119.
[63] K. Zare, N. Shadmani, E. Pournamdari, DFT/NBO study of nanotube and calixarene with anti-cancer drug, J. Nanostruct. Chem. 3 (2013) 75–80.
[64] A. Ahmadi, J. Beheshtian, M. Kamfiroozi, Benchmarking of ONIOM method for the study of NH_3 dissociation at open ends of BNNTs, J. Mol. Model. 18 (2012) 1729–1734.
[65] S. Ghorbaninezhad, M. Ghorbaninezhad, Simulation of nanodrug by theoretical approach, J. Nanostruct. Chem. 3 (2013) 53–60.
[66] S. Tomic, B. Montanari, N.M. Harrison, The group III–V's semiconductor energy gaps predicted using the B3LYP hybrid functional, Phys. E 40 (2008) 2125–2127.
[67] M.W. Schmidt, K.K. Baldridge, J.A. Boatz, S.T. Elbert, M.S. Gordon, J.H. Jensen, S. Koseki, N. Matsunaga, K.A. Nguyen, S. Su, General atomic and molecular electronic structure system, J. Comput. Chem. 14 (1993) 1347–1363.
[68] N.M. O'boyle, A.L. Tenderholt, K.M. Langner, Cclib: a library for package-independent computational chemistry algorithms, J. Comput. Chem. 29 (2008) 839–845.
[69] S.F. Boys, F.d. Bernardi, The calculation of small molecular interactions by the differences of separate total energies. Some procedures with reduced errors, Mol. Phys. 19 (1970) 553–566.
[70] N.L. Hadipour, A. Ahmadi Peyghan, H. Soleymanabadi, Theoretical study on the Al-doped ZnO nanoclusters for CO chemical sensors, J. Phys. Chem. C 119 (2015) 6398–6404.
[71] J. Andzelm, N. Govind, A. Maiti, Nanotube-based gas sensors—role of structural defects, Chem. Phys. Lett. 421 (2006) 58–62.
[72] S. Basu, P. Bhattacharyya, Recent developments on graphene and graphene oxide based solid state gas sensors, Sens. Actuators, B 173 (2012) 1–21.
[73] H. Elhaes, A. Fakhry, M. Ibrahim, Carbon nano materials as gas sensors, Mater. Today: Proc. 3 (2016) 2483–2492.
[74] N.K. Jaiswal, G. Kovačević, B. Pivac, Reconstructed graphene nanoribbon as a sensor for nitrogen based molecules, Appl. Surf. Sci. 357 (Part A) (2015) 55–59.
[75] Y. Li, M. Hodak, W. Lu, J. Bernholc, Mechanisms of NH_3 and NO_2 detection in carbon-nanotube-based sensors: an ab initio investigation, Carbon 101 (2016) 177–183.
[76] J. Beheshtian, M.T. Baei, Z. Bagheri, A.A. Peyghan, Carbon nitride nanotube as a sensor for alkali and alkaline earth cations, Appl. Surf. Sci. 264 (2013) 699–706.
[77] M.T. Baei, A.A. Peyghan, Z. Bagheri, M.B. Tabar, B-doping makes the carbon nanocones sensitive towards NO molecules, Phys. Lett. A 377 (2012) 107–111.
[78] M. Nayebzadeh, A.A. Peyghan, H. Soleymanabadi, Density functional study on the adsorption and dissociation of nitroamine over the nanosized tube of MgO, Phys. E: Low-dimensional Syst. Nanostruct. 62 (2014) 48–54.
[79] J. Li, Y. Lu, Q. Ye, M. Cinke, J. Han, M. Meyyappan, Carbon nanotube sensors for gas and organic vapor detection, Nano Lett. 3 (2003) 929–933.
[80] S. Peng, K. Cho, P. Qi, H. Dai, Ab initio study of CNT NO_2 gas sensor, Chem. Phys. Lett. 387 (2004) 271–276.
[81] Y. Li, N. Chen, D. Deng, X. Xing, X. Xiao, Y. Wang, Formaldehyde detection: SnO_2 microspheres for formaldehyde gas sensor with high sensitivity, fast response/recovery and good selectivity, Sens. Actuators B: Chem. 238 (2017) 264–273.
[82] X. Wang, J. Zhang, L. Wang, S. Li, L. Liu, C. Su, L. Liu, High response gas sensors for formaldehyde based on Er-doped In_2O_3 nanotubes, J. Mater. Sci. Technol. 31 (2015) 1175–1180.
[83] R. Wang, D. Zhang, Y. Zhang, C. Liu, Boron-doped carbon nanotubes serving as a novel chemical sensor for formaldehyde, J. Phys. Chem. B 110 (2006) 18267–18271.
[84] M. Chi, Y.-P. Zhao, Adsorption of formaldehyde molecule on the intrinsic and Al-doped graphene: a first principle study, Comput. Mater. Sci. 46 (2009) 1085–1090.
[85] S.F. Rastegar, A.A. Peyghan, H. Soleymanabadi, Ab initio studies of the interaction of formaldehyde with beryllium oxide nanotube, Phys. E 68 (2015) 22–27.
[86] A. Ahmadi, N.L. Hadipour, M. Kamfiroozi, Z. Bagheri, Theoretical study of aluminum nitride nanotubes for chemical sensing of formaldehyde, Sens. Actuators B: Chem. 161 (2012) 1025–1029.